AUT Journal of Mechanical Engineering

AUT J. Mech. Eng., 1(2) (2017) 149-158
DOI: 10.22060/mej.2017.12281.5303

On the Elastic Field of Al/SiC Nanocomposite

H. Pourhashemi, M. R. Dashtbayazi*

Department of Mechanical Engineering, Faculty of Engineering, Shahid Bahonar University of Kerman, Kerman, Iran

ABSTRACT: This study aims to analyze the linear elastic behavior of an aluminum matrix nanocomposite reinforced with SiC nanoparticles. Once, a representative volume element was considered for the nanocomposite with a cuboidal inclusion. The elastic moduli of the matrix and the inclusion were the same, but it contained eigenstrain. The stress and the strain fields were obtained for the inclusion and the aluminum by Galerkin vector method. The stress and the strain fields in the inclusion problem were in a good agreement with the results in the literature. A similar representative volume element was considered for the nanocomposite with a cuboidal inhomogeneity. The elastic moduli of the matrix and the inhomogeneity were different, but it did not have any eigenstrain. For the calculation of the Eshelby tensor and the elastic fields for the inhomogeneity problem, the equivalent inclusion method (EIM) was applied. In the EIM, the uniform and equivalent eigenstrain were considered. The stress and the strain fields within the inhomogeneity and the matrix were obtained. Results showed that the stress and the strain in the cuboidal inclusion were less than the cuboidal inhomogeneity due to the difference between the matrix and the reinforcement materials.

Review History:

Received: 26 December 2016
Revised: 3 March 2017
Accepted: 7 May 2017
Available Online: 11 September 2017

Keywords:

Nanocomposite
Inclusion
Inhomogeneity
Stress
Strain

1- Introduction

With the increasing application of the nanocomposites in advanced industries, the mechanical behaviors of these materials are important [1]. Nanocomposites are a wide class of composite materials consisting of at least one phase with dimensions in the nanometer scale [2]. As an example, aluminum matrix nanocomposite reinforced with different kinds of ceramic nanoparticles, have been widely used in many engineering fields, because of its remarkable mechanical properties, such as wear resistance, high elastic modulus, high thermal stability, good oxidation and corrosion resistance and fatigue strength [3]. The aluminum matrix nanocomposites have been considered as good candidates, applied as structural materials to the automotive, aerospace and military industries [4]. Many ceramic nanoparticles are used as a reinforcement for the aluminum matrix nanocomposite, namely; Al_2O_3, ZrO_2, MgO, $FeTiO_3$, Si_3N_4, TiC, B_4C, SiC [5]. In this research, we select the SiC as a common reinforcement, because it is inexpensive and accessible.

The nanocomposites are an inhomogeneous material. When a reinforcement is embedded in an elastic matrix, an internal stress field develops inside the reinforcement and the matrix. The reinforcement in the nanocomposite materials disturbs the elastic stress and the strain fields. The disturbance of the stress and the strain fields changes the mechanical behavior of the nanocomposite materials [6]. The calculation of the elastic strain and stress fields existing in the nanocomposites is necessary to characterize the strength, the conditions for fracture, and computation for the critical parameters defects formation. The elastic fields in the nanocomposites depend on many parameters such as the reinforcement and the matrix types, size and shape of the reinforcement, the surface energy of interface, and the matrix and the reinforcement mutual diffusion [7].

In the micromechanical models, the reinforcement as an inclusions in the nanocomposites are represented by an eigenstrain, which are identified with the difference of the matrix and the reinforcement crystal lattices [8]. Generally, the eigenstrain in the micromechanics shows the inelastic strains, namely initial, plastic, thermal, misfit, and phase transformation strains [9]. The eigenstress is caused by one or several of the eigenstrains, which are free from any other external force and surface constraint. We did not consider the concept of the eigenstress in this research. In other words, when the eigenstrain is prescribed in a finite subdomain in a homogenous material, and the eigenstrain is zero in the remainder material (matrix), the subdomain is called the inclusion. When the inclusion is considered, it is assumed the elastic moduli of the material to be homogenous. On the other hand, if the elastic moduli of the subdomain in a material is different from the matrix, then the subdomain is called an inhomogeneity [8].

Mura categorized discontinuous materials into three categories, namely homogeneous inclusions or inclusions, inhomogeneities and inhomogeneous inclusions [9]. The elastic moduli of the homogeneous inclusion or inclusion is similar to the matrix, but it contains the eigenstrain. The elastic moduli of the inhomogeneity is different from the matrix, and it does not have any eigenstrain. Usually, for the calculation of the elastic fields in the inhomogeneity, the equivalent inclusion method (EIM) is applied [9]. In EIM, the uniform eigenstrain was considered due to the difference in the matrix and the reinforcement materials. The inhomogeneous inclusion is an inhomogeneity which contains

Corresponding author, E-mail: dashtbayazi@uk.ac.ir

eigenstrain. Sometimes, the inhomogeneous inclusion is called an inhomogeneous inhomogeneity [8]. The eigenstrain inside the inhomogeneous inclusion are misfit and phase transformation strains [9].

The elastic fields in the nanocomposites are approximated by different approaches. These approaches include the classical linear elasticity [10], atomistic simulations [11], and the combine elastic continuum models with the atomistic simulations [12]. Several analytical solutions have been introduced for the calculation of the linear elastic fields for the inclusions inserted in an infinite medium, like ellipsoidal [13], cuboidal [14], and cylindrical inclusions [15, 16]. The strain field due to a cuboidal inhomogeneity is calculated by Johnson et al. [17, 18]. They applied a polynomial form for equivalent eigenstrain. Eshelby's solution is an important procedure for the calculation of the elastic field for ellipsoidal elastic inclusions in an infinite elastic body with a uniform eigenstrain [19]. The strain gradient effect was not considered by the Eshelby's solution [19]. Ma and Gao considered a strain gradient elasticity theory in the Eshelby problem [20]. Rodin showed that the Eshelby tensor was not constant inside inclusion with polyhedral shape [21]. Also, Rodin explained the Eshelby tensor for polygonal inclusions in two-dimensional space. Nozaki and Taya derived the Eshelby tensor for the polyhedral inclusions in three-dimensional space [22]. Nozaki and Taya calculated the elastic field inside and outside of the regular polyhedral inclusions with different shapes, namely tetrahedron, hexahedron, octahedron, dodecahedron, and icosahedron. Rodin [21] and Nozaki and Taya [22] applied an algorithm developed by Waldvogel [23] for the calculation of the Newtonian potential for the polyhedral inclusions. Kuvshinov presented a compact form for the Eshelby tensor for the polyhedral inclusions [24]. Many analytical solutions were obtained for polyhedral inclusions such as cuboidals by Chiu [25]; Lee and Johnson [26]; Liu and Wang [27], and pyramids by Pearson and Faux [28]; Glas [29]; Nenashev and Dvurechenskil [30].

In this study, the linear elastic behavior of the aluminum matrix reinforced with the SiC nanoparticles is investigated. The shape of the reinforcement is considered cuboidal due to the crystal structure of the SiC [31]. One of the important structure for the SiC is 3C-SiC (β), which we have considered in our research. Like a diamond crystal structure, the crystal structure of 3C-SiC (β) is cubic [32]. The cuboidal SiC is considered once as the inclusion (the inclusion problem) and once again, as the inhomogeneity (the inhomogeneity problem). It is assumed that the SiC nanoparticles are randomly distributed in the aluminum matrix, and the behavior of the nanocomposites are isotropic. The mechanical properties of SiC in a single crystal form is anisotropic [33]. The random distribution of the SiC nanoparticles in the aluminum matrix develops an isotropic condition for Al/SiC nanocomposite. Finally, the stress and the strain distributions of the cuboidal inclusion and inhomogeneity are obtained and the results are compared.

2- Definition of the problems

Fig. 1 shows the representative volume element of the nanocomposite, containing a cuboidal SiC. The SiC reinforcement was considered once as an inclusion. The elastic moduli of the matrix and the inclusion are the same, but the inclusion has eigenstrain. A similar representative volume element for the nanocomposite was considered which contains of the cuboidal inhomogeneity. The elastic moduli of the matrix and the inhomogeneity are different and the inhomogeneity does not have eigenstrain. The aim of the research was finding the stress and the strain distributions in the matrix, the inclusion, and the inhomogeneity.

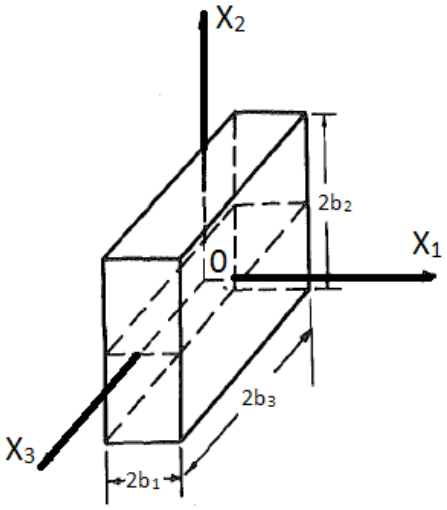

Fig. 1. Cuboidal nanoparticle and Cartesian coordinate with the origin at the centroid

3- Solution to the inclusion problem

In this research, the stress and the strain distributions for the cuboidal inclusion were obtained by the Galerkin vector method [34]. Chiu [14] derived an expression to obtain the stress and the strain fields in an isotropic elastic matrix containing a cuboidal inclusion with the inelastic strains (the eigenstrain) by the Galerkin vector method. Final results of the gradient of displacement parameters are obtained as follows [14]:

$$2\mu u_{i,q} = \frac{1}{8\pi^3}\sum_{n=1}^{8}(-1)^n \begin{bmatrix} \frac{(1-2\nu)}{(1-\nu)}.\lambda\bar{e}_{kk}.D_{,iqmm}(C_n) + 4\mu\bar{e}_{ij}.D_{,jqmm}(C_n) \\ -\frac{2\mu}{1-\nu}\bar{e}_{mj}.D_{,iqmj}(C_n) \end{bmatrix} \quad (1)$$

where λ and μ are the Lame's constants, u_i is displacements vector, and υ is the Poisson's ratio, D is a function of C_n vectors that was introduced in [14], $\bar{e}_{ij}$ is the uniform initial strains inside the inclusion and it is zero outside the inclusion. After the gradients of displacements were calculated by Eq. (1), the elastic components of the strains in the inclusion and the matrix are obtained by [14]:

$$e_{ij} = 1/2\left(u_{i,j} + u_{j,i}\right) - e_{ij}^{'} \quad (2)$$

Then the stresses for the inclusion and the matrix were calculated by the Hooke's law.

4- Solution of the inhomogeneity problem

As mentioned earlier, EIM was applied to calculate the elastic fields for the inhomogeneity problem. The EIM was implemented to calculate the Eshelby tensor for the cuboidal inhomogeneity. The uniform eigenstrain was considered due to the difference in the matrix and the reinforcement materials and temperature variation. Then, the equivalent eigenstrain was calculated. The eigenstrain was added to the total strain

of the inclusion, and then, the strain of the inhomogeneity was calculated. Finally, the stress and the strain distributions were obtained in the inhomogeneity and the matrix.

4- 1- Equivalent inclusion method (EIM)

In EIM, the SiC inhomogeneity simulates as the inclusion within the matrix with an initial eigenstrain ε_{ij}^{p} which adds to an equivalent eigenstrain ε_{ij}^{*} [35]. In EIM, the inhomogeneity in Fig. 2(a) changes into the inclusion in Fig. 2(b). Equivalent eigenstrain ε_{ij}^{*} is a fictitious strain which simulates the perturbation of a stress and strain fields, introduced by the inhomogeneity with different elastic moduli into the applied remote stress. Consequently, equivalent eigenstrains has been defined in order to simulate inhomogeneity problem by the use of the inclusion method [9]. The elastic strains ε_{ij}^{e} in the equivalent inclusions are obtained by [35]:

$$\varepsilon_{ij}^{e} = \varepsilon_{ij} - \varepsilon_{ij}^{*} - \varepsilon_{ij}^{p} \tag{3}$$

where ε_{ij} is the total strain and ε_{ij}^{p} is an initial eigenstrain. According to Hooke's law, Eq. (4) is explained for any point at the equivalent inclusion [35]:

$$\sigma_{ij} = C_{ijkl}\left(\varepsilon_{kl} - \varepsilon_{kl}^{*} - \varepsilon_{kl}^{p}\right) \quad (i,j,k,l = 1,2,3) \tag{4}$$

where σ_{ij} is stress tensor and C_{ijkl} is stiffness tensor.

4- 2- Definition of the polyhedral inhomogeneity

The elastic field in the inhomogeneity with an arbitrary polyhedral shape in an infinite elastic body was calculated by Rodin [21], Nozaki and Taya [22], and Kuvshinov [24]. According to [36], the p-faced polyhedral inclusion is divided into tetrahedral duplexes. Each duplex is divided into two simplexes. Each simplex was considered as a tetrahedron (Fig. 3). The four vertices in each of the duplexes are the projection point of x on a polyhedral surface (i.e., x_I), two adjacent vertices on this surface (i.e., V_{IJ}^{+} and V_{IJ}^{-}), and the point x itself, respectively. A local cartesian coordinate

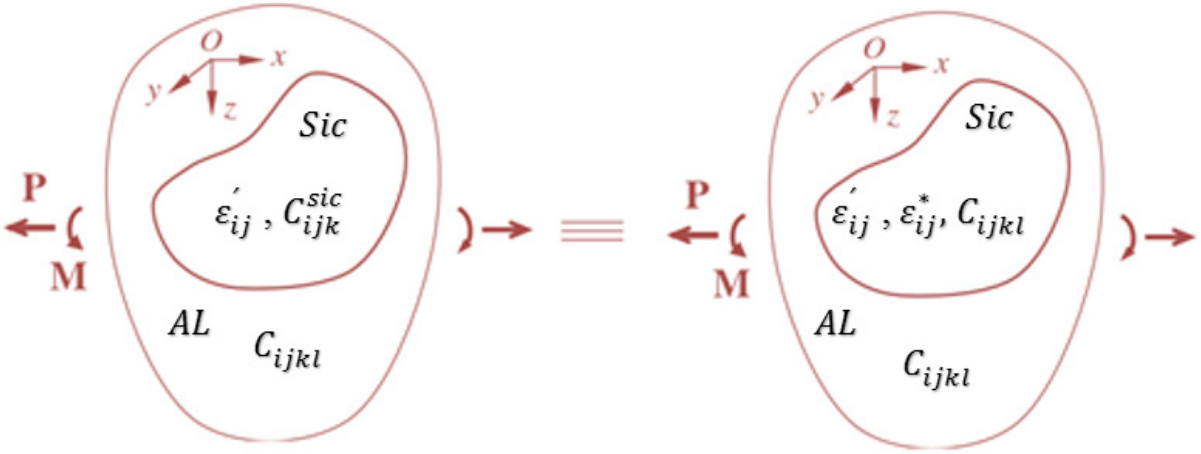

(a) (b)

Fig. 2. Description of the equivalent inclusion method (a) Schematic of SiC arbitrarily shaped inhomogeneity with elastic moduli C_{ijkl}^{SiC} and initial eigenstrain ε_{ij}^{p} embedded in an aluminum matrix with elastic moduli C_{ijkl} (i,j,k,l=1,2,3) under external load, and (b) Using EIM, SiC inhomogeneity in (a) is equivalently treated as an inclusion with ε_{ij}^{p} plus equivalent eigenstrain ε_{ij}^{*} [35].

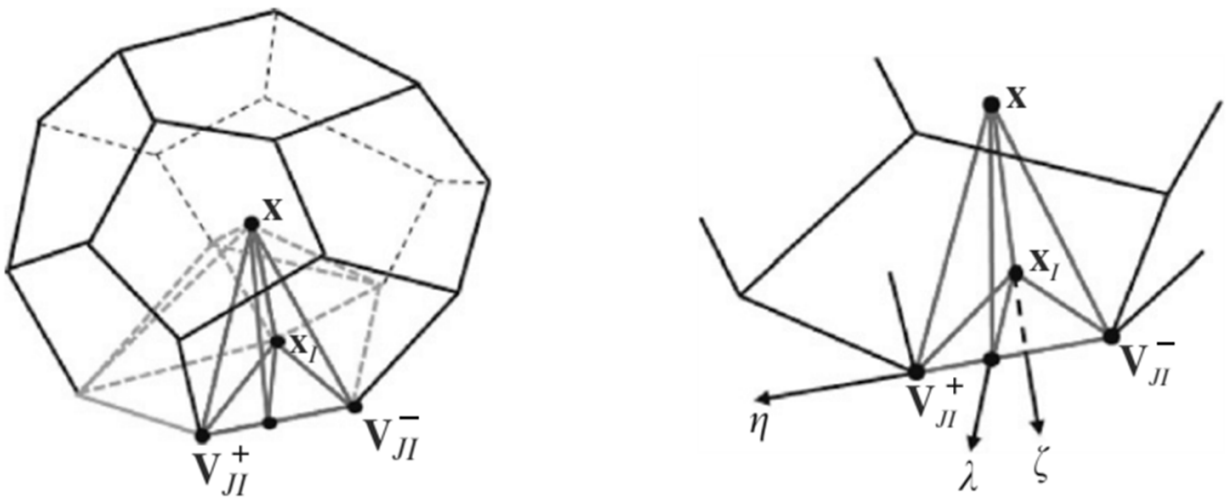

(a) (b)

Fig. 3. A polyhedron represented by duplexes: (a) a polyhedron (with five duplexes shown); (b) a duplex and the associated local coordinate system constructed from an arbitrary point x [36].

system is considered for each duplexes, and point x is considered as the origin. λ, η and ζ are considered as the three orthogonal axes of the local coordinate system. Fig. 4 shows the coordinates of the two vertices V_{IJ}^{+} and V_{IJ}^{-} on the Jth edge of the Ith surface by (b_{JI}, l_{JI}^{+}, a_I) and (b_{JI}, l_{JI}^{-}, a_I). The unit vectors associated with the local coordinates λ, η and ζ are λ_{JI}^{0}, η_{JI}^{0} and ξ_I^{0}. An arbitrary point on the *J*th edge of the *I*th surface is *y*, and the position vector of *y* relative to the origin *x* (i.e., *r*=*y*-*x*) is *r*, and the projection of *r* on the *I*th surface is r_I^s. (x_1, x_2, x_3) are the cartesian coordinates with a (e_1, e_2, e_3) as base vectors.

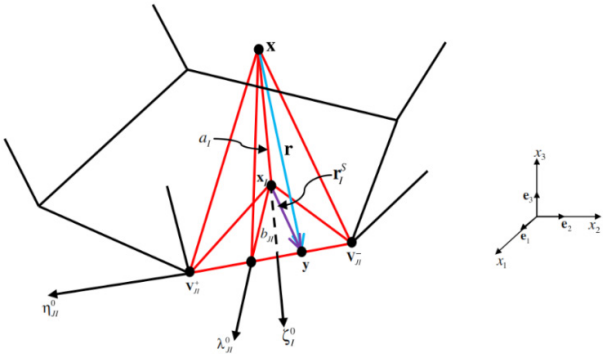

Fig. 4. A duplex with its base on the *I*th surface and one local coordinate axis (η) along the *J*th edge of the Ith surface [36].

4- 3- Calculation of the Eshelby tensor

The Eshelby tensor S_{ijkl} is obtained by two distinct tensors [36]:

$$S_{ijkl} = S_{ijkl}^{C} + S_{ijkl}^{G} \tag{5}$$

$$S_{ijkl}^{C} = \frac{1}{8\pi(1-\nu)}\begin{bmatrix}\Phi_{,ijkl} - 2\nu\Lambda_{,ij}\delta_{kl} \\ -(1-\nu)\left(\Lambda_{,lj}\delta_{ik} + \Lambda_{,kj}\delta_{il} + \Lambda_{,li}\delta_{jk} + \Lambda_{,ki}\delta_{jl}\right)\end{bmatrix} \tag{6}$$

$$S_{ijkl}^{G} = \frac{1}{8\pi(1-\nu)}\begin{bmatrix}2\nu\Gamma_{,ij}\delta_{kl} + (1-\nu)\left(\Gamma_{,jl}\delta_{ik} + \Gamma_{,il}\delta_{jk} + \Gamma_{,jk}\delta_{il} + \Gamma_{,ik}\delta_{jl}\right) \\ +2L^2\left(\Lambda_{,ijkl} - \Gamma_{,ijkl}\right)\end{bmatrix} \tag{7}$$

where, $S_{ijkl}{}^{C}$ and $S_{ijkl}{}^{G}$ are the classical part and the gradient part of Eshelby tensor, respectively, δ_{ij} is the Kronecker delta, and $\Phi(x)$, $\Lambda(x)$ and $\Gamma(x)$ are three scalar-valued potential functions. In order to simplify, in this research, the gradient part of the Eshelby tensor $S_{ijkl}{}^{G}$ is ignored. Finally, the Eshelby tensor is given by:

$$S_{ijkl} = S_{ijkl}^{C} \tag{8}$$

Fig. 5 shows the number of the surfaces for the cuboidal inhomogeneity. According to the definition of the classical Eshelby tensor [22], in Fig. 5, the values of p (i.e. The number of surface) is p=6 and the values of q (i.e. the number of edge in each surface) is q=4. Then, the classical Eshelby tensor from Eq. (8) is given by [36]:

$$\begin{aligned}S_{ijkl}^{c} = \frac{1}{8\pi(1-\vartheta)}\sum_{I=1}^{p}\sum_{J=1}^{q}\Big\{&(S_1^c)_{JI}(\zeta_I^0)_i(\zeta_I^0)_j\delta_{kl} + (S_2^c)_{JI}\left[(\zeta_I^0)_i(\zeta_I^0)_k\delta_{jl} + (\zeta_I^0)_i(\zeta_I^0)_l\delta_{jk}\right] + (S_3^c)_{JI}\left[(\zeta_I^0)_k(\zeta_I^0)_j\delta_{il} + (\zeta_I^0)_l(\zeta_I^0)_j\delta_{ik}\right] + (S_4^c)_{JI}(\zeta_I^0)_i\left(\lambda_{JI}^0\right)_j\delta_{kl} + \\ &(S_5^c)_{JI}\left[(\zeta_I^0)_i\left(\lambda_{JI}^0\right)_k\delta_{jl} + (\zeta_I^0)_i\left(\lambda_{JI}^0\right)_l\delta_{jk}\right] + (S_6^c)_{JI}\left[\left(\lambda_{JI}^0\right)_k(\zeta_I^0)_j\delta_{il} + \left(\lambda_{JI}^0\right)_l(\zeta_I^0)_j\delta_{ik}\right] + (S_7^c)_{JI}(\zeta_I^0)_i\left(\eta_{JI}^0\right)_j\delta_{kl} + (S_8^c)_{JI}\left[(\zeta_I^0)_i\left(\eta_{JI}^0\right)_k\delta_{jl} + (\zeta_I^0)_i\left(\eta_{JI}^0\right)_l\delta_{jk}\right] + (S_9^c)_{JI}\left[\left(\eta_{JI}^0\right)_k(\zeta_I^0)_j\delta_{il} + \left(\eta_{JI}^0\right)_l(\zeta_I^0)_j\delta_{ik}\right] + \\ &(S_{10}^c)_{JI}\left[(\zeta_I^0)_i\left(\lambda_{JI}^0\right)_j(\zeta_I^0)_k(\zeta_I^0)_l + (\zeta_I^0)_i(\zeta_I^0)_j\left(\lambda_{JI}^0\right)_k(\zeta_I^0)_l + (\zeta_I^0)_i(\zeta_I^0)_j(\zeta_I^0)_k\left(\lambda_{JI}^0\right)_l\right] + (S_{11}^c)_{JI}\left[(\zeta_I^0)_i\left(\eta_{JI}^0\right)_j(\zeta_I^0)_k(\zeta_I^0)_l + (\zeta_I^0)_i(\zeta_I^0)_j\left(\eta_{JI}^0\right)_k(\zeta_I^0)_l + (\zeta_I^0)_i(\zeta_I^0)_j(\zeta_I^0)_k\left(\eta_{JI}^0\right)_l\right] + \\ &(S_{12}^c)_{JI}\left[(\zeta_I^0)_i(\zeta_I^0)_j\left(\lambda_{JI}^0\right)_k\left(\lambda_{JI}^0\right)_l + (\zeta_I^0)_i\left(\lambda_{JI}^0\right)_j(\zeta_I^0)_k\left(\lambda_{JI}^0\right)_l + (\zeta_I^0)_i\left(\lambda_{JI}^0\right)_j\left(\lambda_{JI}^0\right)_k(\zeta_I^0)_l\right] + (S_{13}^c)_{JI}\left[(\zeta_I^0)_i(\zeta_I^0)_j\left(\eta_{JI}^0\right)_k\left(\eta_{JI}^0\right)_l + (\zeta_I^0)_i\left(\eta_{JI}^0\right)_j(\zeta_I^0)_k\left(\eta_{JI}^0\right)_l + (\zeta_I^0)_i\left(\eta_{JI}^0\right)_j\left(\eta_{JI}^0\right)_k(\zeta_I^0)_l\right] + \\ &(S_{14}^c)_{JI}\left[(\zeta_I^0)_i\left(\lambda_{JI}^0\right)_j\left(\eta_{JI}^0\right)_k\left(\eta_{JI}^0\right)_l + (\zeta_I^0)_i\left(\eta_{JI}^0\right)_j\left(\lambda_{JI}^0\right)_k\left(\eta_{JI}^0\right)_l + (\zeta_I^0)_i\left(\eta_{JI}^0\right)_j\left(\eta_{JI}^0\right)_k\left(\lambda_{JI}^0\right)_l\right] + (S_{15}^c)_{JI}\left[(\zeta_I^0)_i\left(\eta_{JI}^0\right)_j\left(\lambda_{JI}^0\right)_k\left(\lambda_{JI}^0\right)_l + (\zeta_I^0)_i\left(\lambda_{JI}^0\right)_j\left(\eta_{JI}^0\right)_k\left(\lambda_{JI}^0\right)_l + (\zeta_I^0)_i\left(\lambda_{JI}^0\right)_j\left(\lambda_{JI}^0\right)_k\left(\eta_{JI}^0\right)_l\right] + \\ &(S_{16}^c)_{JI}\left[(\zeta_I^0)_i(\zeta_I^0)_j\left(\lambda_{JI}^0\right)_k\left(\eta_{JI}^0\right)_l + (\zeta_I^0)_i(\zeta_I^0)_j\left(\eta_{JI}^0\right)_k\left(\lambda_{JI}^0\right)_l + (\zeta_I^0)_i\left(\lambda_{JI}^0\right)_j\left(\eta_{JI}^0\right)_k(\zeta_I^0)_l + (\zeta_I^0)_i\left(\lambda_{JI}^0\right)_j(\zeta_I^0)_k\left(\eta_{JI}^0\right)_l + (\zeta_I^0)_i\left(\eta_{JI}^0\right)_j(\zeta_I^0)_k\left(\lambda_{JI}^0\right)_l + (\zeta_I^0)_i\left(\eta_{JI}^0\right)_j\left(\lambda_{JI}^0\right)_k(\zeta_I^0)_l\right]\Big\}\end{aligned} \tag{9}$$

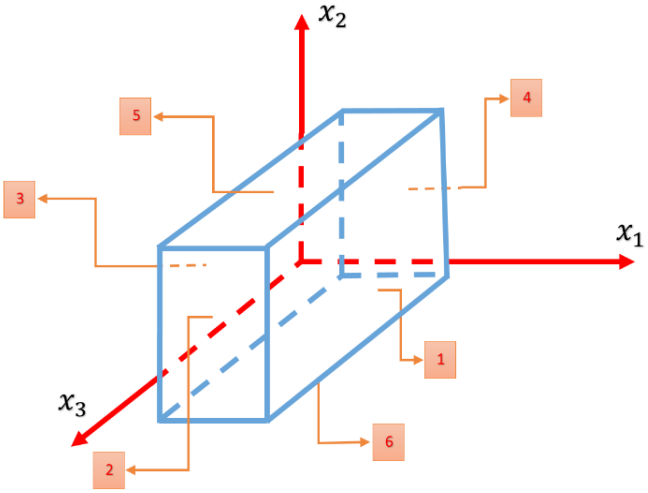

Fig. 5. Number of surfaces in the cuboidal inclusion

The parameters in Eq. (9) are defined as [36]:

$$\begin{aligned}&\left(S_1^c\right)_{JI} = \frac{1}{3}\frac{\partial^3\Phi_1^{JI}}{\partial a_I^3} - 2\vartheta\frac{\partial\Lambda_1^{JI}}{\partial a_I}, \left(S_2^c\right)_{JI} = \frac{1}{3}\frac{\partial^3\Phi_1^{JI}}{\partial a_I^3} - (1-\vartheta)\frac{\partial\Lambda_1^{JI}}{\partial a_I}, \\ &\left(S_3^c\right)_{JI} = -(1-\vartheta)\frac{\partial\Lambda_1^{JI}}{\partial a_I}, \left(S_4^c\right)_{JI} = \frac{1}{3}\frac{\partial^3\Phi_1^{JI}}{\partial b_{JI}^3} - 2\vartheta\frac{\partial\Lambda_1^{JI}}{\partial b_{JI}},\end{aligned} \tag{10}$$

$$\left(S_5^c\right)_{JI}=\frac{1}{3}\frac{\partial^3\Phi_1^{JI}}{\partial b_{JI}^3}-(1-\vartheta)\frac{\partial\Lambda_1^{JI}}{\partial b_{JI}},\left(S_6^c\right)_{JI}=-(1-\vartheta)\frac{\partial\Lambda_1^{JI}}{\partial b_{JI}},$$

$$\left(S_7^c\right)_{JI}=\frac{1}{3}\left[\frac{\partial^3\left(\Phi_1^{JI}\right)^+}{\partial\left(l_{JI}^+\right)^3}-\frac{\partial^3\left(\Phi_1^{JI}\right)^-}{\partial\left(l_{JI}^-\right)^3}\right]-2\vartheta\left[\frac{\partial\left(\Lambda_1^{JI}\right)^+}{\partial l_{JI}^+}-\frac{\partial\left(\Lambda_1^{JI}\right)^-}{\partial l_{JI}^-}\right],$$

$$\left(S_8^c\right)_{JI}=\frac{1}{3}\left[\frac{\partial^3\left(\Phi_1^{JI}\right)^+}{\partial\left(l_{JI}^+\right)^3}-\frac{\partial^3\left(\Phi_1^{JI}\right)^-}{\partial\left(l_{JI}^-\right)^3}\right]-(1-\vartheta)\left[\frac{\partial\left(\Lambda_1^{JI}\right)^+}{\partial l_{JI}^+}-\frac{\partial\left(\Lambda_1^{JI}\right)^-}{\partial l_{JI}^-}\right],$$

$$\left(S_9^c\right)_{JI}=-(1-\vartheta)\left[\frac{\partial\left(\Lambda_1^{JI}\right)^+}{\partial l_{JI}^+}-\frac{\partial\left(\Lambda_1^{JI}\right)^-}{\partial l_{JI}^-}\right],$$

$$\left(S_{10}^c\right)_{JI}=\frac{\partial^3\Phi_1^{JI}}{\partial a_I^2\partial b_{JI}}-\frac{1}{3}\frac{\partial^3\Phi_1^{JI}}{\partial b_{JI}^3},$$

$$\left(S_{11}^c\right)_{JI}=\frac{\partial^3\left(\Phi_1^{JI}\right)^+}{\partial a_I^2\partial l_{JI}^+}-\frac{\partial^3\left(\Phi_1^{JI}\right)^-}{\partial a_I^2\partial l_{JI}^-}-\frac{1}{3}\left[\frac{\partial^3\left(\Phi_1^{JI}\right)^+}{\partial\left(l_{JI}^+\right)^3}-\frac{\partial^3\left(\Phi_1^{JI}\right)^-}{\partial\left(l_{JI}^-\right)^3}\right],$$

$$\left(S_{12}^c\right)_{JI}=\frac{\partial^3\Phi_1^{JI}}{\partial b_{JI}^2\partial a_I}-\frac{1}{3}\frac{\partial^3\Phi_1^{JI}}{\partial a_I^3},$$

$$\left(S_{13}^c\right)_{JI}=\left[\frac{\partial^3\left(\Phi_1^{JI}\right)^+}{\partial\left(l_{JI}^+\right)^2\partial a_I}-\frac{\partial^3\left(\Phi_1^{JI}\right)^-}{\partial\left(l_{JI}^-\right)^2\partial a_I}\right]-\frac{1}{3}\frac{\partial^3\Phi_1^{JI}}{\partial a_I^3},$$

$$\left(S_{14}^c\right)_{JI}=\left[\frac{\partial^3\left(\Phi_1^{JI}\right)^+}{\partial\left(l_{JI}^+\right)^2\partial b_{JI}}-\frac{\partial^3\left(\Phi_1^{JI}\right)^-}{\partial\left(l_{JI}^-\right)^2\partial b_{JI}}\right]-\frac{1}{3}\frac{\partial^3\Phi_1^{JI}}{\partial b_{JI}^3},$$

$$\left(S_{15}^c\right)_{JI}=\frac{\partial^3\left(\Phi_1^{JI}\right)^+}{\partial b_{JI}^2\partial l_{JI}^+}-\frac{\partial^3\left(\Phi_1^{JI}\right)^-}{\partial b_{JI}^2\partial l_{JI}^-}-\frac{1}{3}\left[\frac{\partial^3\left(\Phi_1^{JI}\right)^+}{\partial\left(l_{JI}^+\right)^3}-\frac{\partial^3\left(\Phi_1^{JI}\right)^-}{\partial\left(l_{JI}^-\right)^3}\right],$$

$$\left(S_{16}^c\right)_{JI}=\frac{\partial^3\left(\Phi_1^{JI}\right)^+}{\partial a_I\partial b_{JI}\partial l_{JI}^+}-\frac{\partial^3\left(\Phi_1^{JI}\right)^-}{\partial a_I\partial b_{JI}\partial l_{JI}^-}$$

where I, J are the number of surfaces and the number of the edges in each surface, respectively, functions Φ_I^{JI},$(\Phi_I^{JI})^+$,$(\Phi_I^{JI})^-$ and Λ_I^{JI},$(\Lambda_I^{JI})^+$,$(\Lambda_I^{JI})^-$ in Eq. (10) are defined in Ref. [36]. The parameters a_I, b_{JI}, l_{JI}^+, l_{JI}^- must be obtained where are related to the cuboidal inhomogeneity through Eshelby tensor in Eq. (9) where the parameters a_I, b_{JI}, l_{JI}^+, l_{JI}^- are related to x through [36]:

$$\begin{aligned}a_I&=\left(V_k^+-X_k\right)\left(\zeta_I^0\right)_k,\\ b_{IJ}&=\left(V_k^+-X_k\right)\left(\lambda_{JI}^0\right)_k,\\ l_{JI}^+&=\left(V_k^+-X_k\right)\left(\eta_{JI}^0\right)_k,\\ l_{JI}^-&=\left(V_k^--X_k\right)\left(\eta_{JI}^0\right)_k\end{aligned}\tag{11}$$

The parameters for the surface number one is depicted in Fig. 6.

According to equations in Ref. [36], the parameters a_I, b_{JI}, l_{JI}^+, l_{JI}^- can be calculated as follows:

$$a_1=\left(V_{x_1}^+-X_{x_1}\right)\left(\zeta_I^0\right)_{x_1}+\left(V_{x_2}^+-X_{x_2}\right)\left(\zeta_I^0\right)_{x_2}+\left(V_{x_3}^+-X_{x_3}\right)\left(\zeta_I^0\right)_{x_3}\tag{12}$$

$$\begin{bmatrix}b_{11}\\b_{21}\\b_{31}\\b_{41}\end{bmatrix}=\left(V_{x_1}^+-X_{x_1}\right)\begin{bmatrix}\lambda_{11}^0\\\lambda_{21}^0\\\lambda_{31}^0\\\lambda_{41}^0\end{bmatrix}_{x_1}+\left(V_{x_2}^+-X_{x_2}\right)\begin{bmatrix}\lambda_{11}^0\\\lambda_{21}^0\\\lambda_{31}^0\\\lambda_{41}^0\end{bmatrix}_{x_2}+\left(V_{x_3}^+-X_{x_3}\right)\begin{bmatrix}\lambda_{11}^0\\\lambda_{21}^0\\\lambda_{31}^0\\\lambda_{41}^0\end{bmatrix}_{x_3}\tag{13}$$

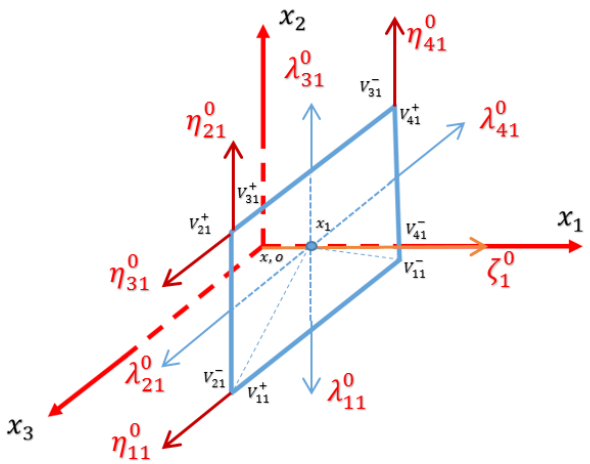

Fig. 6. The parameters of the surface number one for cuboidal inclusion

$$\begin{bmatrix}l_{11}^+\\l_{21}^+\\l_{31}^+\\l_{41}^+\end{bmatrix}=\left(V_{x_1}^+-X_{x_1}\right)\begin{bmatrix}\eta_{11}^0\\\eta_{21}^0\\\eta_{31}^0\\\eta_{41}^0\end{bmatrix}_{x_1}+\left(V_{x_2}^+-X_{x_2}\right)\begin{bmatrix}\eta_{11}^0\\\eta_{21}^0\\\eta_{31}^0\\\eta_{41}^0\end{bmatrix}_{x_2}+\left(V_{x_3}^+-X_{x_3}\right)\begin{bmatrix}\eta_{11}^0\\\eta_{21}^0\\\eta_{31}^0\\\eta_{41}^0\end{bmatrix}_{x_3}\tag{14}$$

$$\begin{bmatrix}l_{11}^-\\l_{21}^-\\l_{31}^-\\l_{41}^-\end{bmatrix}=\left(V_{x_1}^--X_{x_1}\right)\begin{bmatrix}\eta_{11}^0\\\eta_{21}^0\\\eta_{31}^0\\\eta_{41}^0\end{bmatrix}_{x_1}+\left(V_{x_2}^--X_{x_2}\right)\begin{bmatrix}\eta_{11}^0\\\eta_{21}^0\\\eta_{31}^0\\\eta_{41}^0\end{bmatrix}_{x_2}+\left(V_{x_3}^--X_{x_3}\right)\begin{bmatrix}\eta_{11}^0\\\eta_{21}^0\\\eta_{31}^0\\\eta_{41}^0\end{bmatrix}_{x_3}\tag{15}$$

From Fig. 6 for the surface number one, it can be calculated:

$$\left(\zeta_I^0\right)_{x_1}=x_1\ ,\quad\left(\zeta_I^0\right)_{x_2}=0\ ,\quad\left(\zeta_I^0\right)_{x_3}=0\tag{16}$$

$$\begin{aligned}&\left(\lambda_{11}^0\right)_{x_1}=0,\left(\lambda_{11}^0\right)_{x_2}=-x_2,\left(\lambda_{11}^0\right)_{x_3}=0,\\&\left(\lambda_{21}^0\right)_{x_1}=0,\left(\lambda_{21}^0\right)_{x_2}=0,\left(\lambda_{21}^0\right)_{x_3}=x_3\left(\lambda_{31}^0\right)_{x_1}=0,\\&\left(\lambda_{31}^0\right)_{x_2}=x_2,\left(\lambda_{31}^0\right)_{x_3}=0,\left(\lambda_{41}^0\right)_{x_1}=0,\\&\left(\lambda_{41}^0\right)_{x_2}=0,\left(\lambda_{41}^0\right)_{x_3}=-x_3,\end{aligned}\tag{17}$$

$$\begin{aligned}&\left(\eta_{11}^0\right)_{x_1}=0,\left(\eta_{11}^0\right)_{x_2}=0,\left(\eta_{11}^0\right)_{x_3}=x_3,\\&\left(\eta_{21}^0\right)_{x_1}=0,\left(\eta_{21}^0\right)_{x_2}=x_2,\left(\eta_{21}^0\right)_{x_3}=0,\\&\left(\eta_{31}^0\right)_{x_1}=0,\left(\eta_{31}^0\right)_{x_2}=0,\left(\eta_{31}^0\right)_{x_3}=x_3,\\&\left(\eta_{41}^0\right)_{x_1}=0,\left(\eta_{41}^0\right)_{x_2}=x_2,\left(\eta_{41}^0\right)_{x_3}=0\end{aligned}\tag{18}$$

From Eqs. (12) to (18) for the surface number one, the parameters a_I, b_{JI}, l_{JI}^+, l_{JI}^- are calculated as:

$$a_1=\left(b_1-0\right)x_1=b_1x_1\tag{19}$$

$$\begin{aligned}b_{11}&=0+\left(-b_2-0\right)\left(-x_2\right)+0=b_2x_2,\\b_{21}&=0+0+\left(b_3-0\right)x_3=b_3x_3,\\b_{31}&=0+\left(b_2-0\right)\left(x_2\right)+0=b_2x_2,\end{aligned}\tag{20}$$

$$b_{41}=0+0+(-b_3-0)(-x_3)=b_3x_3$$

$$\begin{aligned} l_{11}^{+}&=0+0+(b_3-0)(x_3)=b_3x_3,\\ l_{21}^{+}&=0+(b_2-0)x_2+0=b_2x_2l_{31}^{+}\\ &=0+0+(b_3-0)(x_3)=b_3x_3,\\ l_{41}^{+}&=0+(b_2-0)x_2+0=b_2x_2 \end{aligned} \tag{21}$$

$$\begin{aligned} l_{11}^{-}&=0+0+(-b_3-0)(x_3)=-b_3x_3,\\ l_{21}^{-}&=0+(-b_2-0)x_2+0=-b_2x_2l_{31}^{-}\\ &=0+0+(-b_3-0)(x_3)=-b_3x_3,\\ l_{41}^{-}&=0+(-b_2-0)x_2+0=-b_2x_2 \end{aligned} \tag{22}$$

The details for the calculation of the parameters for other surfaces in Fig. 5 have been described in Ref. [37].
The Eshelby tensor is shown as:

$$S_{ijkl}=\begin{bmatrix} S_{1111} & S_{1122} & S_{1133} & S_{1123} & S_{1131} & S_{1112} & S_{1132} & S_{1113} & S_{1121}\\ S_{2211} & S_{2222} & S_{2233} & S_{2223} & S_{2231} & S_{2212} & S_{2231} & S_{2213} & S_{2221}\\ S_{3311} & S_{3322} & S_{3333} & S_{3323} & S_{3331} & S_{3312} & S_{3332} & S_{3313} & S_{3321}\\ S_{2311} & S_{2322} & S_{2333} & S_{2323} & S_{2331} & S_{2312} & S_{2332} & S_{2313} & S_{2321}\\ S_{3111} & S_{3122} & S_{3133} & S_{3123} & S_{3131} & S_{3112} & S_{3132} & S_{3113} & S_{3121}\\ S_{1211} & S_{1222} & S_{1233} & S_{1223} & S_{1231} & S_{1212} & S_{1232} & S_{1213} & S_{1221}\\ S_{3211} & S_{3222} & S_{3233} & S_{3223} & S_{3231} & S_{3212} & S_{3232} & S_{3213} & S_{3221}\\ S_{1311} & S_{1322} & S_{1333} & S_{1323} & S_{1331} & S_{1312} & S_{1332} & S_{1313} & S_{1321}\\ S_{2111} & S_{2122} & S_{2133} & S_{2123} & S_{2131} & S_{2112} & S_{2132} & S_{2113} & S_{2121} \end{bmatrix} \tag{23}$$

Finally, all parameters for the cuboidal inhomogeneity are substituted into Eq. (6). In our problem, numerical values of the cuboidal inhomogeneity with dimensions $b_1=b_2=b_3=1$ are calculated as:

$$S_{ijkl}=\begin{bmatrix} 0.5959 & 0.0116 & 0.0116 & 0 & 0 & 0 & 0 & 0 & 0\\ 0.0116 & 0.5959 & 0.0116 & 0 & 0 & 0 & 0 & 0 & 0\\ 0.0116 & 0.0116 & 0.5959 & 0 & 0 & 0 & 0 & 0 & 0\\ 0 & 0 & 0 & 0.2021 & 0 & 0 & 0.2021 & 0 & 0\\ 0 & 0 & 0 & 0 & 0.2021 & 0 & 0 & 0.2021 & 0\\ 0 & 0 & 0 & 0 & 0 & 0.2021 & 0 & 0 & 0.2021\\ 0 & 0 & 0 & 0.2021 & 0 & 0 & 0.2021 & 0 & 0\\ 0 & 0 & 0 & 0 & 0.2021 & 0 & 0 & 0.2021 & 0\\ 0 & 0 & 0 & 0 & 0 & 0.2021 & 0 & 0 & 0.2021 \end{bmatrix} \tag{24}$$

4- 4- Calculation of the total strain for the inhomogeneity problem

In EIM, equivalent eigenstrain ε_{ij}^{*} is defined as [35]:

$$\varepsilon_{ij}^{*}=S_{ijkl}e_{ij}^{''} \tag{25}$$

where $e_{ij}^{''}$ is the uniform initial eigenstrain which is due to the difference in temperature and materials and is defined by:

$$e_{ij}^{''}=(\alpha_{Al}-\alpha_{SiC})\delta_{ij}\Delta T \tag{26}$$

where α_{Al} and α_{SiC} are thermal expansion coefficients of the aluminum and the SiC, respectively. δ_{ij} is Kronecker delta and ΔT is the temperature difference. The thermal expansion coefficients of the aluminum and the SiC are $\alpha_{Al}=23.6\times10^{-6}$/°C and $\alpha_{SiC}=4\times10^{-6}$/°C, respectively, and ΔT is the temperature difference between the melting point of the aluminum to environmental temperature (i.e. ΔT=660.32-25=635.32 °C. Then Eq. (26) is calculated by:

$$e_{ij}^{''}=(\alpha_{Al}-\alpha_{SiC})\delta_{ij}\Delta T=(12.452\times10^{-3})\delta_{ij} \tag{27}$$

The equivalent eigenstrain ε_{ij}^{*} is obtained by Eq. (25). All elements of the initial eigenstrain ε_{ij}^{p} are considered zero expect $\varepsilon_{11}^{p}=0.01$,$\varepsilon_{22}^{p}==0.01$,$\varepsilon_{33}^{p}==0.01$, and the total strain is obtained by Eq. (3).

5- Results and Discussion

For the purpose of the model validation, the results of the inclusion problem are compared to the available results by Nozaki and Taya [22]. Fig. 7 shows the results are in a good agreement. Figs. 8 and 9 depict the distribution of the dimensionless stress (σ_{11}/E) for the inclusion problem and the inhomogeneity problem along the dimensionless position (x_1/b_1), respectively. According to results presented in Figs. 8 and 9, the variation of (σ_{11}/E), for the inclusion and the inhomogeneity problem along the axis (x_1/b_1), inside of the inclusion is negative (compression). The variations of (σ_{11}/E), for the inclusion and the inhomogeneity problem along the axis (x_1/b_1), at interface of the inclusion and the inhomogeneity is continuous. Stress outside of the interface for the inclusion tends to be zero. By eliminating the eigenstrain in the inhomogeneity problem, the results of the inclusion problem are obtained. Thus, the results for the inhomogeneity problem are consistent to the inclusion problem.

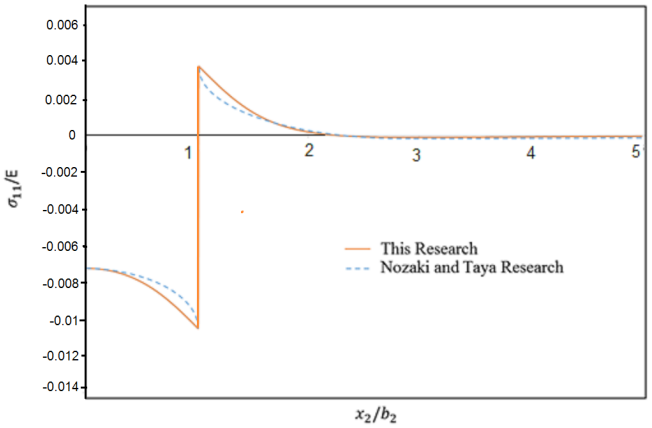

Fig. 7. Comparison of dimensionless stress σ_{11}/E for the inclusion problem with respect to the dimensionless points x_2/b_2 with Nozaki and Taya results [22]

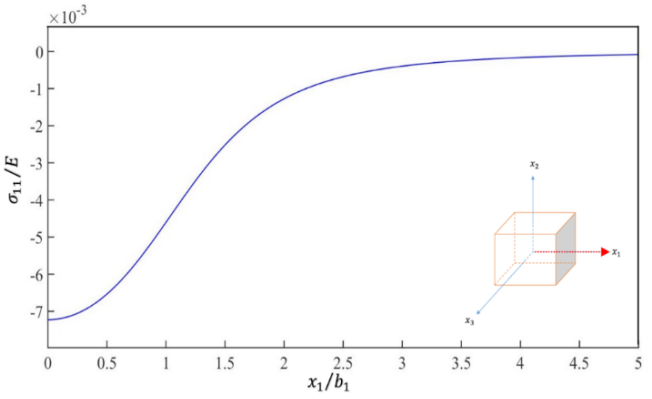

Fig. 8. Distribution of σ_{11}/E for the inclusion problem along the dimensionless position x_1/b_1

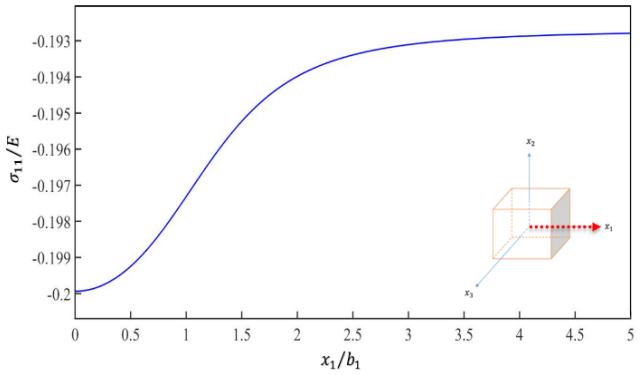

Fig. 9. Distribution of σ_{11}/E for the inhomogeneity problem along the dimensionless position x_1/b_1

Figs. 10 and 11 show the distribution of the dimensionless stress (σ_{11}/E), for the inclusion problem and the inhomogeneity problem along the dimensionless position (x_2/b_2), respectively. According to Figs. 10 and 11, the variation of (σ_{11}/E), for the inclusion and the inhomogeneity problems along the axis (x_2/b_2), inside of the inclusion is compressive. The variations of (σ_{11}/E), for the inclusion and the inhomogeneity along the axis (x_2/b_2), at interface of the inclusion and the inhomogeneity is discontinuous. The variations of the stress at the outside of the interface for the inclusion tend to be zero.

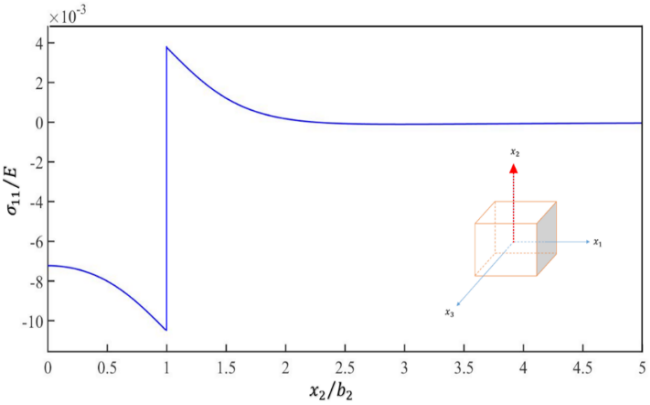

Fig. 10. Distribution of σ_{11}/E for the inclusion problem along the dimensionless position x_2/b_2

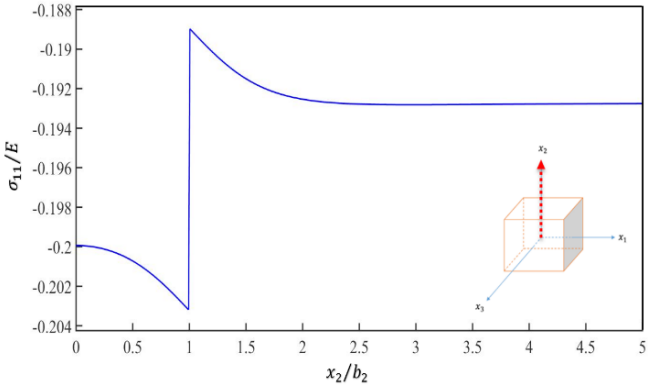

Fig. 11. Distribution of σ_{11}/E for the inhomogeneity problem along the dimensionless position x_2/b_2

Figs. 12 and 13 show the distribution of the dimensionless stress (σ_{11}/E), for the inclusion and the inhomogeneity problems along the dimensionless position (x_3/b_3), respectively.". According to Figs. 12 and 13, the variation of (σ_{11}/E), for the inclusion and the inhomogeneity problems along the axis (x_3/b_3) is similar to the variation of (σ_{11}/E) for the inclusion and the inhomogeneity problems along the axis (x_2/b_2).

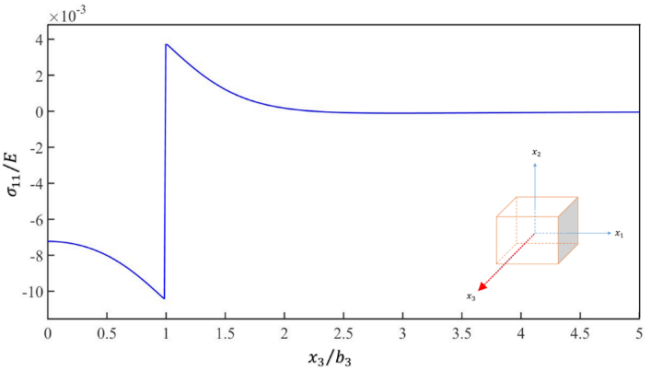

Fig. 12. Distribution of σ_{11}/E for the inclusion problem along the dimensionless position x_3/b_3

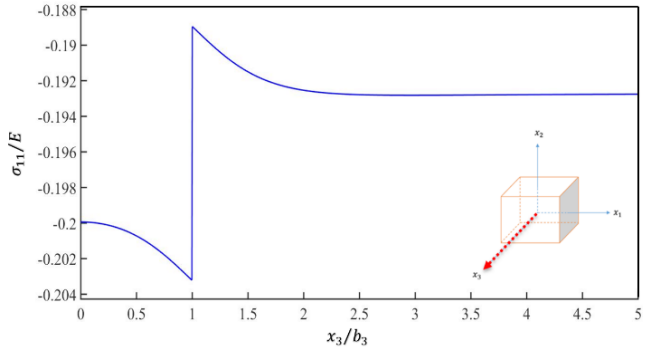

Fig. 13. Distribution of σ_{11}/E for the inhomogeneity problem along the dimensionless position x_3/b_3

Figs. 14 to 19 depict the distribution of the strains for the inclusion and the inhomogeneity problems along the dimensionless axes, respectively. Results show that the distributions of the strains at the interface are discontinuous. Fig. 14 shows that inside the inclusion, the strain ε_{11} is compressive. Although, around the interface of the inclusion, the strain distribution changes from positive (tension) to negative (compression). Fig. 15 shows inside and the outside of the inhomogeneity, the strain ε_{11} is compressive. According to Fig. 16, inside the inclusion, the strain ε_{11} is compressive and outside the inclusion is tensile. Fig. 17 shows the strain distribution in the inside and the outside of the inhomogeneity is compressive. According to Figs. 18 and 19, the variation of the strain ε_{11} for the inclusion and the inhomogeneity problems along the dimensionless position x_3/b_3 is similar to the variation of the strain ε_{11} for the inclusion and the inhomogeneity problems along the dimensionless position x_2/b_2, respectively. Totally, the stress and the strain distributions along the same axes for the inclusion and the inhomogeneity problems have the same trend but the stress and the strain in the inclusion problem is less than the inhomogeneity problem due to the difference between

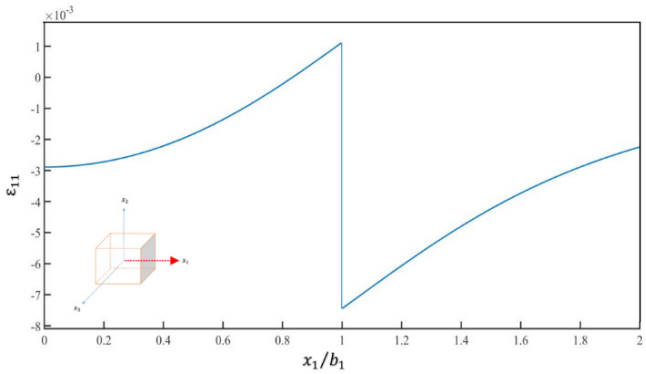

Fig. 14. Distribution of strain ε_{11} for the inclusion problem along the dimensionless position x_1/b_2

properties of reinforcement and matrix materials.

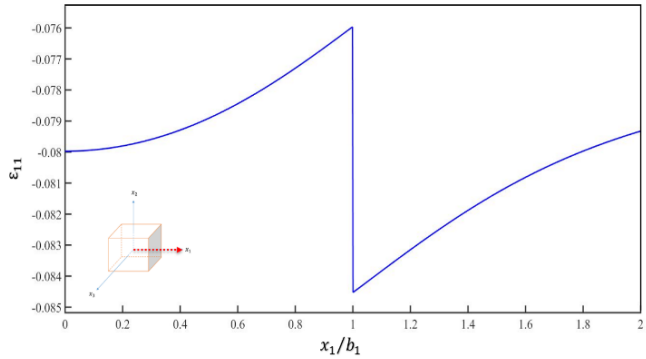

Fig. 15. Distribution of strain ε_{11} for the inhomogeneity problem along the dimensionless position x_1/b_2

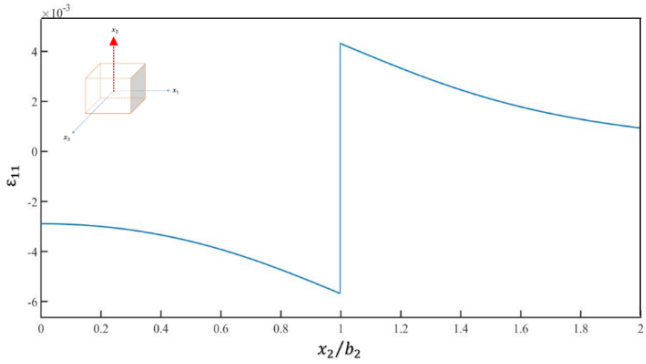

Fig. 16. Distribution of strain ε_{11} for the inclusion problem along the dimensionless position x_2/b_2

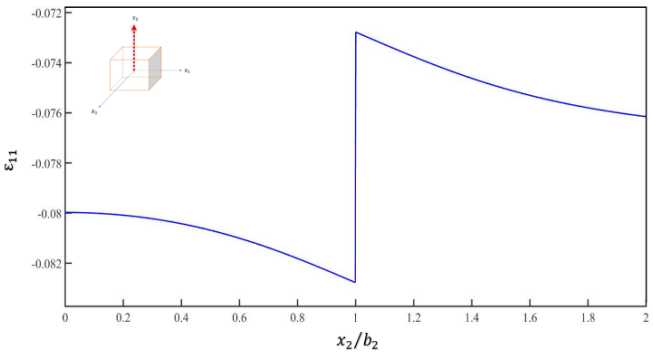

Fig. 17. Distribution of strain ε_{11} for the inhomogeneity problem along the dimensionless position x_2/b_2

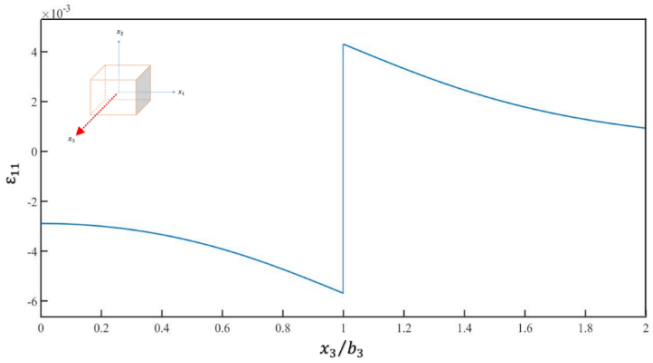

Fig. 18. Distribution of strain ε_{11} for the inclusion problem along the dimensionless position x_3/b_3

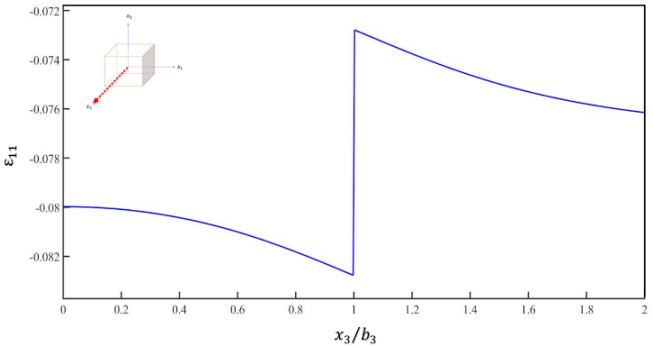

Fig. 19. Distribution of strain ε_{11} for the inhomogeneity problem along the dimensionless position x_3/b_3

6- Conclusion

The linear elastic behavior of the aluminum matrix reinforced with the SiC nanoparticles was analyzed. Two representative volume elements for the nanocomposite were considered, one for the cuboidal inclusion and the other for the cuboidal inhomogeneity. The stress and the strain distributions were found for the inclusion problem by the Galerkin vector method, and for the inhomogeneity problem by the equivalent inclusion method (EIM). The major outcomes of this study were:

- The variations of the dimensionless stress (σ_{11}/E) for the inclusion and inhomogeneity problems along the dimensionless position (x_1/b_1), at the interface of the inclusion and the inhomogeneity was, continuous.
- The variations of the dimensionless stress (σ_{11}/E) for the inclusion and the inhomogeneity problems along the dimensionless position (x_2/b_2), at the interface of the inclusion and the inhomogeneity was, discontinuous.
- The distributions of the strains at the interface of the inclusion and the inhomogeneity were discontinuous.
- The stresses and strains distributions along the same axes for the inclusion and the inhomogeneity problems had the same trend but the stresses and strains in the inclusion problem were less than the inhomogeneity problem due to the differenece between mechanical properties of matrix and reinforcement materials.

References

[1] D. Vollath, D.V. Szabó, Synthesis and properties of nanocomposites, *Advanced Engineering Materials*, 6(3) (2004) 117-127.

[2] P.M. Ajayan, L.S. Schadler, P.V. Braun, *Nanocomposite science and technology*, Wiley-VCH, 2003.

[3] Y. Yang, J. Lan, X. Li, Study on bulk aluminum matrix nano-composite fabricated by ultrasonic dispersion of nano-sized SiC particles in molten aluminum alloy, *Materials Science and Engineering: A*, 380(1–2) (2004) 378-383.

[4] C. Borgonovo, D. Apelian, M.M. Makhlouf, Aluminum nanocomposites for elevated temperature applications, *JOM*, 63(2) (2011) 57-64.

[5] [5] R. Casati, Vedani, M., Metal Matrix Composites Reinforced by Nano-Particles—A Review, Metals, 4 (2014) 65-63.

[6] J. Bernholc, D. Brenner, M. Buongiorno Nardelli, V. Meunier, C. Roland, Mechanical and electrical properties of nanotubes, *Annual Review of Materials Research*, 32(1) (2002) 347-375.

[7] I. Ovidko, A. Sheinerman, Elastic fields of inclusions in nanocomposite solids, *Reviews on Advanced Materials Science*, 9 (2005) 17-33.

[8] J. Qu, M. Cherkaoui, *Fundamentals of Micromechanics of Solids*, Wiley, Hoboken, New Jersey, 2006.

[9] T. Mura, *Micromechanics of Defects in Solids*, 2nd ed., Springer, Netherlands, 1987.

[10] L. Tian, Rajapakse, R.K.N.D., Analytical solution for size-dependent elastic field of a nanoscale circular inhomogeneity, *ASME Journal of Applied Mechanics* 74, 568–574, (2007).

[11] J.A. Zimmerman, E.B. WebbIII, J.J. Hoyt, R.E. Jones, P.A. Klein, D.J. Bammann, Calculation of stress in atomistic simulation, Modelling and Simulation in Materials Science and Engineering, 12(4) (2004) S319.

[12] J.-L. Tsai, S.-H. Tzeng, Y.-T. Chiu, Characterizing elastic properties of carbon nanotubes/polyimide nanocomposites using multi-scale simulation, *Composites Part B: Engineering*, 41(1) (2010) 106-115.

[13] J.D. Eshelby, The determination of the elastic field of an ellipsoidal inclusion, and related problems, in: Proceedings of the Royal Society of London A: Mathematical, Physical and Engineering Sciences, *The Royal Society*, 1957, pp. 376-396.

[14] Y.P. Chiu, On the Stress Field Due to Initial Strains in a Cuboid Surrounded by an Infinite Elastic Space, *Journal of Applied Mechanics*, 44(4) (1977) 587-590.

[15] L. Wu, S. Du, The Elastic Field Caused by a Circular Cylindrical Inclusion—Part I: Inside the Region $x12 + x22 < a2, -\infty < x3 < \infty$ Where the Circular Cylindrical Inclusion is Expressed by $x12 + x22 \le a2, -h \le x3 \le h$, *Journal of Applied Mechanics,* 62(3) (1995) 579-584.

[16] L. Wu, S.Y. Du, The Elastic Field Caused by a Circular Cylindrical Inclusion—Part II: Inside the Region $x12 + x22 > a2, -\infty < x3 < \infty$ Where the Circular Cylindrical Inclusion is Expressed by $x12 + x22 \le a2, -h \le x3 \le h$, *Journal of Applied Mechanics*, 62(3) (1995) 585-589.

[17] W.C. Johnson, Y.Y. Earmme, J.K. Lee, Approximation of the Strain Field Associated With an Inhomogeneous Precipitate—Part 1: Theory, *Journal of Applied Mechanics*, 47(4) (1980) 775-780.

[18] W.C. Johnson, Y.Y. Earmme, J.K. Lee, Approximation of the Strain Field Associated With an Inhomogeneous Precipitate—Part 2: The Cuboidal Inhomogeneity, *Journal of Applied Mechanics*, 47(4) (1980) 781-788.

[19] J.D. Eshelby, The Elastic Field Outside an Ellipsoidal Inclusion, Proceedings of the Royal Society of London. *Series A. Mathematical and Physical Sciences*, 252(1271) (1959) 561-569.

[20] H. Ma, X.-L. Gao, Eshelby's tensors for plane strain and cylindrical inclusions based on a simplified strain gradient elasticity theory, *Acta mechanica*, 211(1-2) (2010) 115-129.

[21] G.J. Rodin, Eshelby's inclusion problem for polygons and polyhedra, *Journal of the Mechanics and Physics of Solids* 44, 1977-1995, (1996).

[22] H. Nozaki, M. Taya, Elastic fields in a polyhedral inclusion with uniform eigenstrains and related problems, *Journal of Applied Mechanics, Transactions ASME* 68, 441-452, (2001).

[23] J. Waldvogel, The Newtonian potential of homogeneous polyhedra, *Zeitschrift für Angewandte Mathematik und Physik* 30, 388-398, (1979).

[24] B.N. Kuvshinov, Elastic and piezoelectric fields due to polyhedral inclusions, *International Journal of Solids and Structures* 45, 1352-1384., (2008).

[25] Y.P. Chiu, On the stress field due to initial strains in a cuboid surrounded by an infinite elastic space, *Journal of Applied Mechanics, Transactions ASME* 44, 587-590, (1977).

[26] J.K. Lee, W.C. Johnson, Calculation of the elastic strain field of a cuboidal precipitate in an anisotropic matrix, *physica status solidi* (a), 46(1) (1978) 267-272.

[27] S. Liu, Q. Wang, Elastic Fields due to Eigenstrains in a Half-Space, *Journal of Applied Mechanics*, 72(6) (2005) 871-878.

[28] G.S. Pearson, D.A. Faux, Analytical solutions for strain in pyramidal quantum dots, *Journal of Applied Physics*, 88(2) (2000) 730-736.

[29] F. Glas, Elastic relaxation of truncated pyramidal quantum dots and quantum wires in a half space: An analytical calculation, *Journal of Applied Physics*, 90(7) (2001) 3232-3241.

[30] A.V. Nenashev, A.V. Dvurechenskii, Strain distribution in quantum dot of arbitrary polyhedral shape: Analytical solution, *Journal of Applied Physics*, 107(6) (2010) 064322.

[31] C.B. Carter, M.G. Norton, *Ceramic Materials: Science and Engineering*, Springer, 2007.

[32] M. Takahiro, K. Yoshitake, Y. Taku, S. Naoki, A. Jun, Superconductivity in carrier-doped silicon carbide, *Science and Technology of Advanced Materials*, 9(4) (2008) 044204.

[33] G.L. Harris, INSPEC, Properties of Silicon Carbide, INSPEC, *Institution of Electrical Engineers*, 1995.

[34] Y.C. Fung, X. Chen, P. Tong, Classical and Computational Solid Mechanics (Second Edition), World Scientific Publishing Company Pte Limited, 2016.

[35] K. Zhou, L.M. Keer, Q.J. Wang, Semi-analytic solution for multiple interacting three-dimensional inhomogeneous inclusions of arbitrary shape in an infinite space, *International Journal for Numerical Methods in Engineering*, 87(7) (2011) 617-638.

[36] X.L. Gao, M.Q. Liu, Strain gradient solution for the Eshelby-type polyhedral inclusion problem, *Journal of the Mechanics and Physics of Solids*, 60(2) (2012) 261-276.

[37] S.H. Pourhashemi, *Analysis of the linear elastic behaviour of the aluminum matrix nanocomposite reinforced with silicon carbide nanoparticles*, Shahid Bahonar University of Kerman, (2015).

Please cite this article using:

H. Pourhashemi and M. R. Dashtbayazi, On the Elastic Field of Al/SiC Nanocomposite, *AUT J. Mech. Eng.*, 1(2) (2017) 149-158.

DOI: 10.22060/mej.2017.12281.5303